PHYSICAL REVIEW B VOLUME 49, NUMBER 20 15 MAY 1994-II

Quantum size dependence of femtosecond electronic dephasing and vibrational dynamics in CdSe nanocrystals

D. M. Mittleman*
Materials Sciences Division, Lawrence Berkeley Laboratory, 1 Cyclotron Road, MS 70-193A, Berkeley, California 94720
and Department of Physics, University of California, Berkeley, California 94720

R. W. Schoenlein
Materials Sciences Division, Lawrence Berkeley Laboratory, 1 Cyclotron Road, MS 70-193A, Berkeley, California 94720

J. J. Shiang and V. L. Colvin
Department of Chemistry, University of California, Berkeley, California 94720

A. P. Alivisatos
Materials Sciences Division, Lawrence Berkeley Laboratory, 1 Cyclotron Road, MS 70-193A, Berkeley, California 94720
and Department of Chemistry, University of California, Berkeley, California 94720

C. V. Shank
Materials Sciences Division, Lawrence Berkeley Laboratory, 1 Cyclotron Road, MS 70-193A, Berkeley, California 94720;
Department of Physics, University of California, Berkeley, California 94720;
and Department of Chemistry, University of California, Berkeley, California 94720

(Received 10 January 1994)

Femtosecond photon-echo techniques are used to probe the dynamics of quantum-confined excitons in nanocrystals of CdSe. Using three-pulse photon echoes, the modulation of the echo signal from the LO-phonon mode is effectively suppressed, and both the electronic dephasing and the couplings to lattice vibrations are probed directly. Detailed measurements are reported as a function of both nanocrystal size and temperature. The dephasing times vary from 85 fs in nanocrystals of 20-Å diameter to 270 fs in 40-Å crystals. These rates are determined by several dynamical processes, all of which depend sensitively on the size of the nanocrystal. The time scale of the trapping of the electronic excitation to surface states increases with increasing size. The coupling of the excitation to low-frequency vibrational modes is strongly size dependent as well, in accordance with a theoretical model. The photon echo also gives information on the polar coupling between the electronic state and the LO-phonon mode. This coupling is found to peak at an intermediate size. This phenomenon is interpreted as a manifestation of coupling between the interior confined excitons and localized surface states, which destroys the spherical symmetry of the excited state. Using these data, all of the important contributions to the size-dependent homogeneous linewidths can be enumerated.

I. INTRODUCTION

In the last decade, nanocrystals of metallic, semiconductor, and insulator materials have been the subject of intense scrutiny. Numerous experimental and theoretical efforts have been made to understand the electronic, optical, and structural properties of these materials. The excitement surrounding these nanostructured systems stems in part from their potential use in electronic or optoelectronic devices.[1] It has long been known that an exciton confined to two dimensions, as in a semiconductor quantum well, exhibits enhanced oscillator strength and enhanced nonlinear optical properties compared to the bulk (i.e., unconfined) exciton.[2-4] An exciton confined in all three spatial dimensions is interesting not only because of its greatly enhanced optical nonlinearities,[5] but also because it is a prototypical system for investigating the physics of quantum confinement. Three-dimensional confinement strongly influences the homogeneous absorption line shape of the exciton, as well as the strengths of the exciton-lattice couplings. The ultrafast electronic and vibrational dynamics of nanocrystalline systems can give direct information about the evolution of these physical properties as a function of size.

A simple calculation predicts that in a semiconductor nanocrystal with a diameter smaller than or comparable to the exciton Bohr radius, the quantum confinement energy is larger than the Coulomb interaction energy (or exciton binding energy).[6] Thus the energy required to create a "quantum-confined exciton" in a nanocrystal is substantially larger than the band gap of the bulk crystal, varying roughly as $E_{\text{gap}} \sim 1/R^2$. In realistic systems, the shift of the quasiexciton peak due to the confinement can be as large as 1 eV.[6,7] The quantum confinement is also manifest in a loss of translation symmetry; as a consequence, the continuous bulk band structure evolves into a series of discrete molecular transitions. The absorption widths of these transitions are much broader than typical molecular linewidths.[8] In recent years, a considerable number of experimental studies have attempted to determine the origins of this broadening. A natural distinction can be drawn between those broadening mechanisms which are intrinsic to *any* quantum-confined semiconductor and those mechanisms which depend on other factors such as the nature of the nanocrystal surface passivation or the host matrix. Unfortunately, experimental determinations of the relative importance of these mechanisms have been complicated by issues such as the broad size dispersions present in the samples. As a result, little is known about the nature of couplings which lead to intrinsic natural linewidths in highly quantum-confined systems.

Recent advances in the fabrication of nanocrystals of CdS and CdSe,[9-11] silicon,[12] germanium,[13] and continued work on the synthesis of GaAs (Refs. 14 and 15) have facilitated investigations of the fundamental properties of the electronic states of highly confined semiconductors. One can now study in great detail how these properties evolve as the solid shrinks continuously toward a molecular limit. In the II-VI compounds CdS and CdSe, the range of sizes currently accessible by chemical synthesis allows one to study how electronic wave functions and their couplings to lattice vibrations change as the number of atoms increases from only a few hundred to many thousands. Numerous spectral hole burning[8,16-21] and luminescence[18,22-26] experiments have been performed in order to determine the homogeneous linewidth of the lowest excited state. Resonance Raman techniques[27-30] have been used to probe the coupling of the electronic excitation to the optical-phonon mode of the crystal. These experiments as well as electroabsorption measures[31,32] have provided important details about the shape of the excited-state wave functions. Femtosecond optical techniques have been used to investigate the excited-state dynamics, such as the ultrafast surface trapping, through time-resolved absorption saturation measurements.[18,33-35] Because of the extreme sensitivity of the energy of the lowest state to the size of the nanocrystal, even the most monodisperse samples exhibit inhomogeneously broadened absorption spectra.[18-36] This fact has complicated the interpretation of many of these measurements. While it is known that a number of distinct mechanisms may contribute to the homogeneous linewidth of individual nanocrystals, the relative importance and size dependence of these mechanisms is not well understood.

In this paper we present femtosecond photon-echo measurements performed on nanocrystals of CdSe. This technique avoids the issue of inhomogeneous broadening in the samples because the integrated photon-echo signal reflects the average properties of all of the nanocrystals within the inhomogeneous distribution.[37] CdSe has a vibrational (phonon) mode at ~210 cm^{-1} which is strongly coupled to the electronic excitation; this phonon mode complicates the interpretation of two-pulse echo experiments, and requires the use of a three-pulse (or stimulated) photon echo. Using three-pulse techniques to suppress the modulation of the echo signal by the phonon mode, we can separately measure both the electronic dephasing due to scattering or relaxation processes and the dynamics of the lattice vibrations.[38] By modeling the data using well-established descriptions of the femtosecond four-wave mixing process, we can extract quantitative information about the exciton–optical-phonon coupling, the exciton dephasing time, and the surface trapping time. We also report the first quantitative measurements of the size-dependent coupling of the exciton to the heat bath of low-frequency or "acoustic" modes.

II. EXPERIMENT

The nanocrystals used in these experiments are grown at ~350 °C in trioctyl phosphine oxide (TOPO).[9,10] A tributyl phosphine precursor solution of dimethyl cadmium and selenium is injected into the hot solvent, causing the rapid formation of nucleation sites and subsequent growth of crystalline CdSe. Rapid quenching of the growth is achieved by cooling the solution. Coagulation of the nanocrystals is prevented by the TOPO itself, which binds to the nanocrystal surfaces ($<25\%$ coverage[39]) and inhibits contact between crystals by steric hindrance. A small quantity (~30 mg) of nanocrystals in powdered form is subsequently obtained by precipitation in methanol. X-ray powder diffraction, transmission electron microscopy, and linear optical spectroscopy are used to determine the mean particle diameter, the size dispersion, and the degree of crystallinity.[9,10,40] The variation in particle diameter ($\pm 5\%$) leads to an inhomogeneous half-width of ~600 cm^{-1} in typical samples. These samples maintain the (bulk) wurtzite crystal structure over the whole range of sizes. TEM and x-ray studies indicate that there is, on average, fewer than one crystalline stacking fault per nanocrystal.[10] For the optical measurements, the nanocrystals are uniformly dispersed in a free-standing polymer (polyvinyl butyral, PVB) film of ~200-μm thickness, which is mounted in a cryostat with optical access. Figure 1 shows the low-temperature (10 K) optical-absorption spectra of several of the nanocrystal samples used in this work. The distinct peak in each spectrum arises from transitions into the lowest-energy quasiexcitonic states. The absorption spectra also exhibit peaks at higher energies, which are evidence of higher excited states. Although the spectra of Fig. 1 have been scaled for clarity, the optical density (OD) of all samples used in these experiments is ~0.2–0.3 OD at the peak of the lowest excited state. These absorption spectra are not observed to change dramatically with age if the samples are stored in a dark, oxygen-free environment.

The larger nanocrystals (30-Å diameter and larger) are studied using a laser system based on the colliding-pulse mode-locked (CPM) ring dye laser. The CPM pulses are amplified at 8 kHz by a copper vapor laser (CVL) in a six-pass dye amplifier (Rhodamine 640),[41] and then coupled into a short (8–10 mm) length of single-mode optical fiber in order to broaden the pulse spectrum.[42] These broadened pulses are then amplified by a second CVL in a four-pass amplifier [DCM/Rhodamine B (Ref. 43)] and

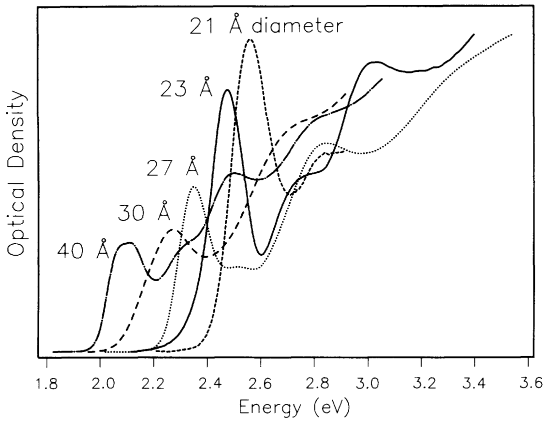

FIG. 1. Low-temperature (10 K) linear-absorption spectra of several samples of CdSe nanocrystals. Mean particle diameters are shown. These spectra have been scaled for clarity.

compressed using gratings and prisms.[42] In order to insure that the pulse spectrum overlaps only the lowest excited state of the nanocrystals, it is necessary to window the pulse spectrum by placing an iris between the second and third prisms. This increases the measured pulse width by approximately a factor of 2, depending on the width of the spectral window. The resulting laser pulses are 20–25 fs in duration, and tunable from ~565 to ~630 nm (~1.97 to ~2.2 eV).

A laser system designed to produce femtosecond pulses in the blue-green spectral regime is used to study the smaller nanocrystals ($\leq$30-Å diameter). This laser system also starts with amplified CPM pulses, but in this case a XeF excimer laser pumps the amplifier at 400 Hz.[44] These pulses, amplified to ~1 μJ per pulse, are used to generate a white-light continuum in ethylene glycol. This continuum is then injected into a second dye amplifier pumped by the same excimer laser. The bandwidth of the amplified light is determined either by an interference filter after the ethylene glycol or by the gain bandwidth of the dye (or dye mixture) in the second amplifier. The relatively well-behaved chirp of the continuum generation process allows for subsequent compression of these pulses to 15–20-fs duration using gratings and prisms.[44] These laser pulses have central wavelengths from ~475 to ~560 nm (~2.2 to ~2.6 eV), depending on the dye(s) used in the second amplifier.

The spectrum of the laser is tuned to the red side of the low-temperature absorption peak of the sample under study, in order to avoid exciting higher-lying transitions. The details of the electronic structure of these materials are complicated by the finite confining potential, the nonparabolic nature of the valence band, and the influence of surface electronic states. Recent theoretical descriptions of the electronic states of CdSe nanocrystals have incorporated the complicated valence-band structure,[45] although the structure of the surface states remains poorly understood. These theories indicate that the dominant contribution to the excitonic absorption peak is the lowest-energy transition ($1S_{F=3/2}-1S_e$, following the notation of Ref. 45), although the $2S_{3/2}-1S_e$ electronic transition also contributes a small fraction (~10%). Higher-lying transitions are at sufficiently higher energies that they do not contribute to the excitonic peak. The femtosecond photon-echo experiment measures a dephasing rate which is an average over all of the electronic states excited by the laser, weighted by their oscillator strengths. Therefore, we expect that these measurements reflect primarily the dephasing dynamics of the lowest-energy electronic excited state.

In CdSe nanocrystals as in bulk semiconductors the energy of the lowest excited state shifts with temperature. When measuring photon-echo signals as a function of temperature, we first obtain absorption spectra at both room temperature and at 10 K, to confirm that over the entire temperature range studied the laser is always resonant with the lowest excitonic peak but never pumping the higher-lying states. In order to insure that there are no systematic effects arising from this tuning of the line with temperature, we have measured photon-echo signals at a fixed temperature while tuning the laser pulse spectrum within the inhomogeneous absorption band of the sample. The photon-echo response does not depend significantly on the position of the laser relative to the peak of the absorption, as long as the laser stays within the inhomogeneously broadened absorption band, sufficiently separated from the higher-lying transitions.

The integrated three-pulse photon-echo is detected in a direction $(-\mathbf{k}_1+\mathbf{k}_2+\mathbf{k}_3)$ determined by phase matching. This spatial direction is symmetric under interchange of $\mathbf{k}_2$ and $\mathbf{k}_3$, and consequently the roles of the beams with these wave vectors can be exchanged. However, the temporal delays of these two laser pulses are not interchangeable. The optically prepared state of the system is a coherent polarization in the time interval between the first and second pulses, and a population state in the interval between the second and third pulses. As a result, the photon-echo signal behaves quite differently when measured as a function of the second-pulse delay (t_{12}) than when measured as a function of the third-pulse delay (t_{13}). The three-pulse photon echo is therefore an excellent tool for investigating both polarization and population dynamics.

In all experiments, we verify that the photon-echo signal exhibits the expected I^3 dependence on laser intensity. This is achieved with a laser fluence on the order of 0.2 mJ/cm^2 per excitation beam, which corresponds to roughly 0.1 photons per nanocrystal. These experiments are in the perturbative limit, where density-matrix descriptions of the nonlinear susceptibility $\chi^{(3)}$ are valid.

III. THEORY

In a previous paper,[38] we showed that time-resolved four-wave mixing experiments in a system such as the nanocrystals are complicated by strong coupling to a single vibrational mode. This mode, at ~210 cm^{-1}, corresponds to the bulk LO phonon in CdSe. The first laser pulse initiates coherent nuclear motion at the phonon frequency which modulates the polarization and the related echo signal. This quantum beat can lead to a surprisingly fast decay of a photon-echo signal, which is *not* a result of fast electronic dephasing. One can separate the effects of electronic dephasing from the effects of nuclear motion by performing a three-pulse photon echo. The integrated echo signal can be measured as a function of the delay of the second pulse (t_{12}) or the delay of the third pulse (t_{13}). If the third-pulse delay is chosen to coincide with exactly one vibrational period (~ 160 fs), then the nuclei are in their initial equilibrium positions and the echo signal as a function of t_{12} reflects only the electronic dephasing. In this fashion, one can suppress the effects of the vibrational mode on the echo signal. Alternatively, one can measure the dynamics of the population grating modulated by the nuclear motion, simply by measuring the echo signal as a function of t_{13}. In fact, for $t_{12}=0$, the echo signal as a function of t_{13} is a direct measure of the population decay, and contains the same information as a pump-probe signal. Thus the three-pulse echo can be used to measure the electronic dephasing, the population (or lifetime) dynamics, and the dynamics of the vibrational mode.

The utility of the three-pulse echo technique in suppressing the effects of a single-frequency oscillator has been known for some time in the fields of nuclear magnetic resonance and electron-spin resonance.[46] Similar experiments have been performed using much longer optical pulses.[47] The mode suppression technique has been recently applied on the femtosecond time scale to the study of inverse micelle CdSe nanocrystals[38] and large organic molecules in solution.[48]

The decay of the integrated photon-echo signal in an inhomogeneous medium can be calculated using a density-matrix formalism. The response of an ideal two-level system is well known: the integrated echo signal as a function of t_{12} decays exponentially with a time constant given by $T_2/4$, where $(T_2)^{-1}=(\tau_D)^{-1}+(2T_1)^{-1}$; here τ_D is the pure electronic dephasing time of the medium, and T_1 is the excited-state lifetime. In the presence of one or more coupled vibrations, the situation is somewhat more complex. One can describe these dynamics with a mixed formalism, in which the perturbative density-matrix treatment is retained for the electronic degrees of freedom, and the nuclear motion is described by the creation and propagation of vibrational wave packets on the ground- and excited-state potential surfaces.[49,50] This formalism has been discussed extensively in the literature in recent years,[51,52] and has proved useful in the interpretation of both time-domain and frequency-domain four-wave mixing experiments.[53]

The calculation of the three-pulse echo signal within this formalism is a straightforward extension of the work of Yan and Mukamel.[52] The underlying assumptions include the rotating wave approximation and the Condon approximation, which are used to write the third-order polarization in terms of Green-function propagators on the nuclear potential surfaces. These surfaces are assumed to be offset harmonic oscillators. For an inhomogeneously broadened two-level system coupled to a single harmonic mode at frequency ω, the integrated photon-echo signal in the direction $-\mathbf{k}_1+\mathbf{k}_2+\mathbf{k}_3$ is given by

$$\begin{aligned} S(t_{12},t_{13}) \sim \exp\{ & -4\Delta^2[n(\omega)+\tfrac{1}{2}] \\ & \times(1-\cos\omega t_2)(1-\cos\omega t_{13})\} \\ & \times\exp[-4t_{12}/T_2]\exp[-2t_{13}/T_1] \\ & \times\Phi(t_{12},t_{13})\ , \end{aligned} \qquad (1)$$

where $n(\omega)$ is the Bose occupation factor, $n(\omega)=[\exp(\hbar\omega/k_BT)-1]^{-1}$, and Δ parameterizes the coupling between the electronic state and the harmonic mode. This dimensionless parameter corresponds to the offset between the ground- and excited-state nuclear harmonic potentials, and is expressed in units of the zero point motion. If the nuclear motion corresponds to an optical-phonon mode, then $\frac{1}{2}\Delta^2$ is equal to the Huang-Rhys parameter. In this expression, the laser pulses are assumed to be δ functions in time, given by $E_1(t)\sim E_0\delta(t)$, $E_2(t)\sim E_0\delta(t-t_{12})$, and $E_3(t)\sim E_0\delta(t-t_{13})$.

The function $\Phi(t_{12},t_{13})$ is given by

$$\begin{aligned} \Phi(t_{12},t_{13})=1+\cos[\Delta^2\{ & \sin(\omega t_{12})-\sin(\omega t_{13}) \\ & +\sin(\omega t_{13}-\omega t_{12})\}]\ . \end{aligned} \qquad (2)$$

This term arises from the interference between different Liouville space pathways.[52,56] We note that $\Phi(t_{12},t_{13})=1$ for either $\omega t_{12}=2\pi$ or $\omega t_{13}=2\pi$. In general, however, this interference term cannot be neglected.

The modulation of the echo signal described by Eq. (1) corresponds to the harmonic motion of the nuclei $\delta x\sim\Delta[1-\cos(\omega t)]$, where $\delta x=0$ corresponds to the equilibrium position in the ground state (i.e., before excitation). Clearly, the modulation of the echo is completely suppressed when $t_{13}=2\pi/\omega$, $4\pi/\omega$, etc. Then the signal as a function of t_{12} reduces to the simple two-level system result. This form of the echo signal [Eqs. (1) and (2)] can also be derived using the time-dependent wave-packet propagation formalism of Heller.[54]

Figure 2 shows the calculated three-pulse echo

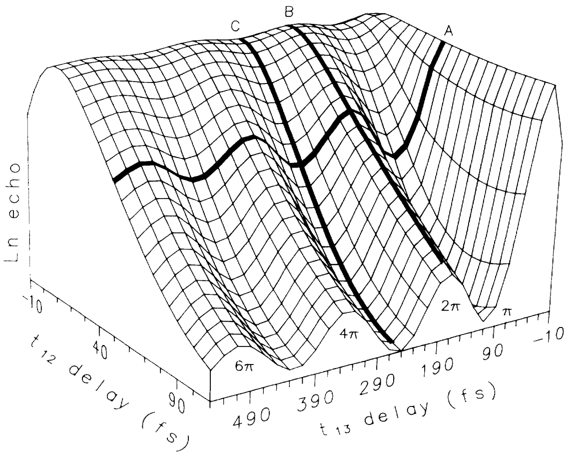

FIG. 2. Calculated three-pulse photon-echo signal for a two-level system coupled to a single vibrational mode at a frequency of 205 cm^{-1}, as a function of the delay between pulses 1 and 2 (t_{12}) and 1 and 3 (t_{13}). The calculation is plotted on a natural log scale. Solid line A corresponds to $t_{12}=50$ fs. Solid lines B and C correspond to $t_{13}=170$ and 250 fs.

response in the presence of a single vibrational mode, as a function of the pulse delays t_{12} and t_{13}. This illustrative calculation includes a dephasing time of 80 fs and a vibrational mode at 205 cm^{-1}, as well as realistic pulses (i.e., finite duration) and finite inhomogeneous broadening. The solid line labeled A represents the echo response as a function of the third pulse delay for a fixed delay of the second pulse ($t_{12}=50$ fs). The oscillations in A result from the vibrational coherence of the LO phonon excited by the first laser pulse. This calculation also includes the damping of this vibrational motion as measured by resonance Raman techniques.[27] A damping time of 700 fs, corresponding to a Raman fundamental linewidth of 15 cm^{-1}, has been included in this simulation. This damping is incorporated in the simulation via a Langevin equation for the nuclear motion.[55,56] As a result of the damping, the nuclei never return entirely to their equilibrium positions. Since the electronic polarization is modulated by the nuclear motion, the vibrational dynamics are not completely decoupled from the electronic dephasing. The damping of the vibrational motion contributes a small but measurable amount to the electronic dephasing. In a single mode system, if the mode has a damping parameter γ [corresponding to the full width at half-maximum (FWHM) of the Raman line], then the contribution to electronic dephasing (at absolute zero) is $(\tau_{\mathrm{damp}})^{-1}=\frac{1}{2}\gamma\Delta^2$.[56] For a damping time of 700 fs and a coupling strength of $\Delta=0.7$, this corresponds to $\tau_{\mathrm{damp}}\sim 2.8$ ps.

Lines B and C in Fig. 2 show explicitly how the suppression effect acts in a single-mode system. By delaying the third pulse by one vibrational period ($t_{13}=2\pi/\omega$), the effects of the quantum beat on the echo signal are suppressed (curve B). Conversely, if the third pulse is positioned out of phase with the oscillation ($t_{13}=3\pi/\omega$), the effects of the quantum beat are enhanced, and the echo signal decays rapidly (curve C). The modulation of the polarization is again suppressed when $\omega t_{13}=4\pi,6\pi,\ldots$. However, we expect that the suppression will be less effective at longer t_{13} delays, for two reasons. First, as explained above, the vibrational damping is an additional contribution to dephasing which increases with increasing t_{13}. Second, previous work has shown[18,23,33] that the exciton created by an optical excitation traps on a fast (ps or faster) time scale to a highly localized surface state. This lifetime (T_1) effect is manifested by a fast initial decay of the population grating. This decay is superimposed on the oscillations, and leads to a faster echo decay at longer third-pulse delays. This trapping mechanism is not necessarily distinct from the vibrational damping. It is possible that some component of the vibrational damping is a result of the fast surface trapping, since the surface localization may significantly perturb the excited-state charge distribution, and thereby dephase the coherent nuclear motion. However, we have no direct evidence for a dynamical process of this type, and no good theory to describe it. As a result, for the purposes of our analysis, we have separated the two effects. We expect that the decay of the echo signal at $t_{13}=2\pi/\omega$ will be slower than the decay at any other third-pulse delay, and will be the most accurate measure of the electronic dephasing. The additional contributions (lifetime and vibrational damping) can accurately be measured by detecting the echo signal as a function of t_{13}.

In order to model this surface trapping process, we must modify Eq. (1) to describe a three-level system, in which the third level is nearly isoenergetic with the excited state, and only weakly optically coupled to the ground state. This can be accomplished simply by replacing the lifetime decay term $\exp\{-2t_{13}/T_1\}$ by the expression $[(1-\alpha)+\alpha\exp\{-t_{13}/T_1\}]^2$, where α represents the fractional recovery of the bleach signal. If the third level is "dark" (that is, has zero oscillator strength with the ground state), then $\alpha=\frac{1}{2}$, reflecting the fact that the excited state becomes depopulated as the trapping occurs, but the ground state does not recover any population.[57] By incorporating this phenomenological description into the model, we can accurately reproduce all of the important features of the experimental data. The mode-suppressed echo, when combined with the excited-state lifetime as measured from the decay of the population grating (echo as a function of t_{13} with $t_{12}=0$), is sufficient to determine both T_1 and T_2, as well as the vibrational damping time of the LO phonon.

We extract the various parameters (e.g., T_1, T_2, Δ, τ_{damp}, etc.) by simulating the results using a calculation based on the theoretical models of Mukamel[55,56] and Pollard.[49] This formalism describes any nonlinear optical spectroscopy in terms of four different three-time correlation functions, which are evaluated by propagation of vibrational wave packets on multidimensional ground- and excited-state nuclear potential surfaces. The third-order polarization is then expressed in terms of a triple-time integral of these correlation functions. In the case of offset (by Δ) harmonic potential surfaces with equal frictional damping coefficients on the ground and excited states, the three-time correlation functions $R_i(t_3,t_2,t_1)$ ($i=1,\ldots,4$) can be written as a sum of single-time correlation or "line-shape" functions $g(t)$,[53,56] thus greatly simplifying the calculation. This result also follows from a second-order cumulant expansion.[52] The model easily incorporates the effects of finite laser pulse duration, nonideal temporal or spectral laser pulse profiles, finite sample temperature, and finite inhomogeneous absorption width. This numerical model has been used to generate the data of Fig. 2, as well as the fits to the data shown in Figs. 3 and 7. The model calculation of Fig. 2 assumes an infinite excited-state lifetime, but the fits to the data in Figs. 3 and 7 use finite values of T_1 and α, as determined from the observed population dynamics.

IV. RESULTS AND DISCUSSION

A. Population dynamics

Figure 3 shows the three-pulse photon-echo signal (measured at 15 K) as a function of the third-pulse delay, with the first two pulses overlapped (i.e., $t_{12}=0$ fs). In this configuration, the echo is a direct measure of the population dynamics, and the signal decays with a func-

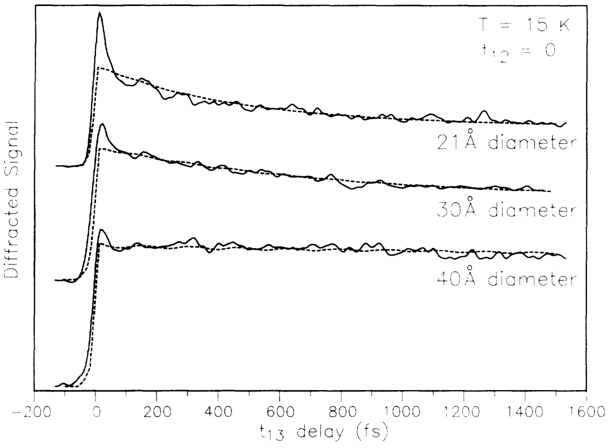

FIG. 3. Three-pulse photon-echo signal (at 15 K) as a function of t_{13} with $t_{12}=0$ fs, for several different samples. Dashed lines are numerical simulations using the model described in the text. The parameters describing the lifetime decays are $T_1=540$ fs, $\alpha=0.38$ (top curve, 21 Å), $T_1=900$ fs, $\alpha=0.23$ (middle curve, 30 Å), and $T_1=8.2$ ps, $\alpha=0.15$ (bottom curve, 40 Å). Mean particle diameters are shown. These data have been vertically offset, for clarity.

tional form which is the square of the decay observed in a pump-probe measurement. The data show a partial recovery of the bleach signal to a constant level, which subsequently remains unchanged for at least tens of picoseconds, the limit of our measurements. The time scale of this partial recovery is strongly dependent on the size of the nanocrystals. The numerical simulations (dashed curves) indicate that this time constant ranges from 0.4 ps in the smallest samples to roughly 8 ps in the largest. This indicates that the initially prepared state changes to some other electronic configuration which has a smaller oscillator strength. The size dependence of this process suggests that a surface trapping mechanism may be responsible. Rapid (10 ps) surface trapping times have been reported in one size of CdS nanocrystals.[23] Fast trapping to localized surface states has been discussed by several authors,[18,22,58] although the detailed nature of these states remains poorly understood. If the trapping process is driven by wave-function overlap between the initial state and the surface, then the trapping rate should vary roughly as the surface-to-volume ratio. A summary of the measured lifetimes is presented in Fig. 11 (the × symbols), along with a best fit to a $1/R$ dependence. The fractional recovery of the bleach (the parameter α discussed above) decreases monotonically with increasing particle size, from approximately 40% to 15%. This suggests that the change in oscillator strength between the initially prepared electronic configuration and the surface trapped state is largest in the smallest nanocrystals. This result is consistent with recent measurements of the electric-field-modulated luminescence, in which the change in the dipole moment between the absorbing and emitting states was determined to decrease with increasing diameter.[59]

B. Coherent nuclear motion

If the first two pulses are separated in time ($t_{12}>0$ fs), the population dynamics are modulated by the coherent LO-phonon mode. Figure 4 shows the three-pulse photon-echo signal (measured at 15 K) as a function of the third-pulse delay, with the second pulse fixed at $t_{12}=33$ fs. This particular value of t_{12} is chosen as a compromise. For $t_{12}=0$, the coherent nuclear motion has a small but noticeable effect, as seen in the top (21 Å) trace of Fig. 3. As t_{12} increases, the contrast ratio of the oscillations increases, but the overall signal level declines exponentially, since the polarization dephases at a rate proportional to $\exp\{-t_{12}/T_2\}$ (see Fig. 2). The value of $t_{12}=33$ fs is long enough so that the oscillations are clearly visible, but not so long that the signal has decayed beyond the dynamic range of the measurement. These data can be qualitatively compared with curve *A* of Fig. 2. We clearly observe oscillations arising from the coherent vibrational excitation, with a period of ~160 fs. This matches the frequency of the LO phonon measured by resonance Raman.[27] In addition, we observe that the size and apparent damping time of these oscillations are functions of the diameter of the nanocrystal. By subtracting the slowly decaying background and fitting the data to an exponentially damped sinusoid, we can extract the damping times of the oscillations. These damping times are shown in Fig. 5. Also shown are the resonance Raman linewidths measured on the same types of nanocrystals by Shiang, Grubbs, and Alivisatos.[13] The data clearly show a strong decrease in the damping time with size, consistent with observations in CdS.[28]

There are several possible explanations for the observed size dependence of the phonon damping time. It is possible that different nanocrystals throughout the sample have slightly different LO-mode frequencies, due to differences in the shapes or sizes of the individual particles. These different frequencies would beat against one another, leading to an apparent decay of the amplitude of

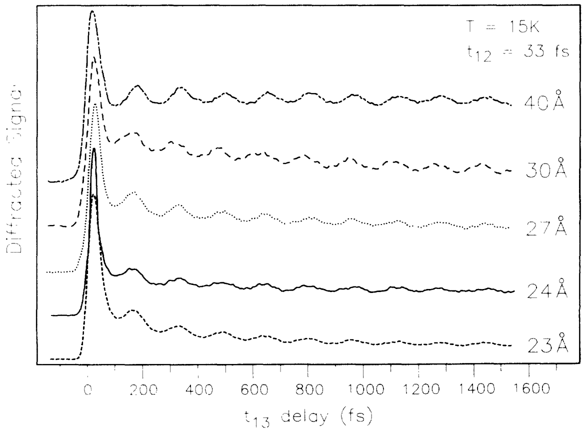

FIG. 4. Three-pulse photon-echo signal (at 15 K) as a function of t_{13} with $t_{12}=33$ fs, for several different samples. Mean particle diameters are shown. These data have been vertically offset, for clarity.

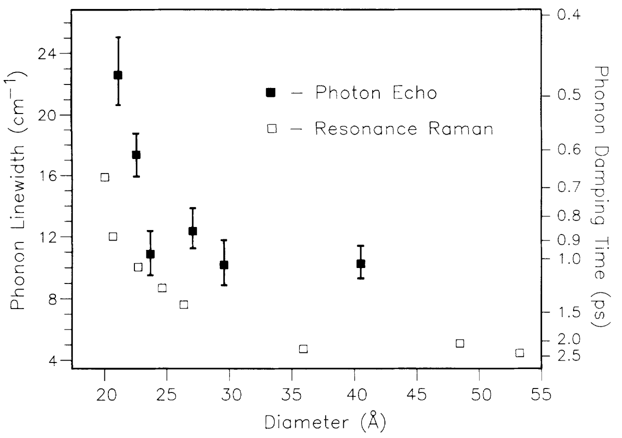

FIG. 5. Damping time of the phonon oscillations as a function of mean particle diameter. The equivalent FWHM of the decay is shown on the left axis. Also shown are the FWHM of the resonance Raman 1-LO peaks, from Ref. 13.

the oscillations. This mechanism would also lead to an inhomogeneously broadened Raman line. It should be noted that the frequency of the LO mode has been observed to shift slightly with nanocrystal size in CdSe.[13] However, this shift is small, amounting to only $\sim 5\ \mathrm{cm}^{-1}$ from bulk CdSe down to 20-Å diameter. This $\Delta\omega$ corresponds to a damping time of greater than 2 ps, which is slower than any of the damping times we have measured. Thus, it is not possible to attribute the Raman linewidth to an inhomogeneous distribution of particle sizes. Given that the width changes monotonically with size, we can also rule out the possibility of an inhomogeneous distribution of particle shapes.

Another possible mechanism for the damping is enhanced anharmonicity of the nuclear potential surface. In smaller nanocrystals, a larger fraction of the constituent atoms reside on the surface, and are therefore not tetrahedrally coordinated. This breakdown of the crystal symmetry leads to anharmonic contributions to the phonon coordinate, which is larger in smaller nanocrystals. However, this model also predicts that the temperature dependence of the resonance Raman linewidth is stronger in smaller nanocrystals. Detailed studies of the Raman linewidths in nanocrystals of CdS have contradicted this prediction.[28] Similar investigations of the linewidths in CdSe nanocrystals have been less unambiguous,[13] but they nonetheless indicate that the temperature dependence is not a strong function of size. For this reason, we conclude that the anharmonic coupling, while possibly contributing significantly to the linewidth, does not change dramatically with size.

The damping of the phonon oscillations is more accurately described by a multimode picture of the confined vibration. This model has been used to understand Raman linewidths in CdS nanocrystals.[28] In the simplest picture, the range of allowed oscillation frequencies in a given nanocrystal ($\Delta\omega$) is determined by the spread in wave vector Δq through the (bulk) phonon-dispersion curve $\omega = \omega(q)$, according to $\Delta\omega = |d\omega(q)/dq|_{q=q_0}\Delta q$. Because of the curvature of $\omega(q)$, the magnitude of the derivative increases for increasing wave vector. The confinement is manifest in the value of q_0, which is inversely proportional to the radius of the nanocrystal. As a consequence, smaller nanocrystals have larger $\Delta\omega$ for fixed Δq. Thus, in smaller nanocrystals, there are a larger number of allowed vibrational frequencies, and as a result the phonon oscillations are more strongly damped. A more detailed analysis would include effects such as the phonon density of states and the confined phonon wave vector.

The mechanism which gives rise to the lifetime effect observed in Fig. 3 could also contribute to the vibrational damping. It is plausible that the fast change in the excited-state wave function causes a partial loss of vibrational coherence. If this were the case, we would expect to observe a decay in the amplitude of the oscillations on the same time scale as the surface trapping. This decay would correspond to the loss of vibrational coherence of the excited-state nuclear wave packet. However, the oscillatory signal has contributions from both the ground-state (impulsive stimulated Raman scattering) and excited-state nuclear wave packets. Thus we would expect a fast contribution to the damping from the excited-state dynamics, as well as a slow contribution from the ground state. However, the fast decay has a time constant which is not much longer than one vibrational period, and we are unable to observe this effect. Nevertheless, this dynamical process may be the origin of the difference between the resonance Raman linewidths measured by Shiang, Grubbs, and Alivisatos[13] and our photon-echo measurements. In a system with fast electronic dephasing, the resonance Raman experiment is primarily a probe of ground-state vibrational motion, and is insensitive to the vibrational dynamics on the excited state.[60] The surface trapping mechanism would not affect the resonance Raman linewidth, because it is intrinsically an excited-state effect. However, the photon echo is sensitive to the vibrational motion in both the ground *and* excited states,[52,61] and is therefore affected by any loss of vibrational coherence arising from surface trapping.

C. Polarization dephasing

Figure 6 shows the three-pulse photon-echo signal (measured at 15 K) as a function of t_{12}, with $\omega t_{13} = 2\pi$, to suppress the effects of the phonon mode. At small delay times, the signal shows a fast (pulsewidth limited) response, which is followed by a slower exponential decay. The fast component at early delays is not well understood. It is not explained by the two-level model used to simulate these data. This model includes all eight terms in the third-order perturbation expansion, including those terms which contribute to coherent coupling effects. Nonetheless, these calculations do not predict a fast response at these early times. It is possible that additional coherent coupling terms arising from the multilevel nature of the electronic spectrum could explain this phenomenon. Alternatively, a bimodal distribution of nanocrystals could give rise to a biexponential polarization decay. This fast response could be an indication of

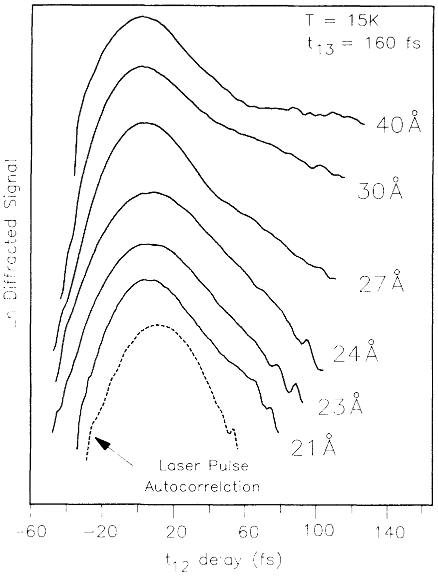

FIG. 6. Three-pulse photon-echo signal (at 15 K) as a function of t_{12} and $t_{13}=160$ fs$\approx 2\pi/\omega$, for several different samples. The signals are plotted on a natural log scale, and mean particle diameters are shown. These data have been vertically offset for clarity. Also shown is an autocorrelation of a 15-fs laser pulse at a wavelength of 500 nm. The slope of the falling edge of this autocorrelation function is a rough measure of the system resolution.

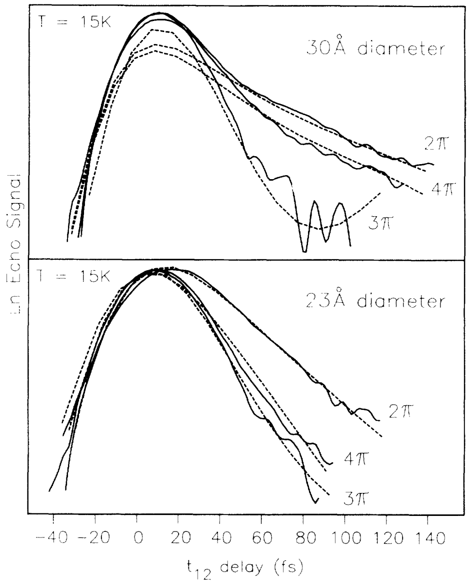

FIG. 7. Three-pulse photon-echo signal (at 15 K) as a function of t_{12} with $\omega t_{13}=2\pi$, 3π, and 4π, corresponding to third-pulse delays alternating in and out of phase with the quantum beat. The signals are plotted on a natural log scale, and two different sizes of nanocrystal are shown. The dashed lines are numerical simulations of the data, using the model discussed in the text. These simulations use the parameters from the second and fifth lines of Table I.

dynamics which are too fast for us to resolve. In any event, the fast response is only present at very early delays ($t_{12}<40$ fs), when the first two pulses are overlapped in the sample. As a matter of course, we only interpret the data at delays long enough to insure that the pulses are not temporally overlapped. For $t_{12}>40$ fs, we observe approximately linear echo decays (on a natural log scale), and the echo decay rate is a strong function of the diameter of the nanocrystals. There are several important mechanisms which contribute to the polarization dephasing, all of which depend on the size of the nanocrystals.[62] The measurements described here allow us to disentangle these various mechanisms.

Figure 7 shows the mode suppression effect in two different samples of nanocrystals. This figure shows the echo signal (on a natural log scale) as a function of t_{12}, with the third pulse fixed at $\omega t_{13}=2\pi$, 3π, and 4π. The modulation of the echo signal by the quantum beat is clearly evident in the alternating fast and slow echo decays. Note that the recovery of the signal $\omega t_{13}=4\pi$ relative to the $\omega t_{13}=2\pi$ trace is more complete in the larger nanocrystals. This is a reflection of the fact that both the vibrational damping and the T_1 (or lifetime) effect are slower in the larger samples.

By observing the contrast between the echo decay rate at $\omega t_{13}=2\pi$ and at $\omega t_{13}=3\pi$, we can extract the exciton–LO-phonon-coupling parameter (Δ) as a function of particle diameter. In principle, one could also obtain this information by directly fitting the oscillations shown in Fig. 4. However, by fitting t_{12} data such as those shown in Fig. 7, we are only comparing the differences in two echo decay rates, without relying on the accuracy of the signal near zero delay. This is therefore a more accurate method of measuring Δ.

We have performed numerical simulations of the t_{12} data at various third-pulse delays, and optimized the fits in order to extract the parameters T_2 and Δ. Samples of these fits are shown in Fig. 7, and a summary of the results are given in Table I. The nonmonotonic behavior of Δ with size is somewhat surprising. In one of the earliest treatments of exciton-phonon coupling in semiconductor nanocrystals, Schmitt-Rink, Miller, and Chemla[63] predicted that, due to the enhanced overlap between the electron and hole, the polar Frölich coupling to the LO-

TABLE I. Mean nanocrystal diameters in Å, dephasing times (T_2) in femtoseconds, and LO-phonon coupling parameters (Δ) for the six samples studied. T_2 and Δ were extracted from three-pulse photon-echo signals as discussed in the text. The CdSe bulk values for T_2 and Δ are from Refs. 78 and 62, respectively.

Mean diameter (Å)	T_2 (fs)	Δ
21.2	85	0.5
22.6	95	0.55
23.7	110	0.55
27.1	130	0.6
29.6	210	0.7
40.5	270	0.65
bulk CdSe	50 ps	0.63

phonon mode would decrease monotonically as the size of the nanocrystal decreases. Other more detailed theoretical efforts have predicted no size dependence in this size regime,[29] or a decrease with size followed by a monotonic increase in coupling strength as the nanocrystals shrink below ~100-Å diameter.[64] It is interesting to note that all of these theories describe the eigenstates of the nanocrystal using centrosymmetric wave functions, in accordance with ideal spherical boundary conditions. The experimentally observed behavior is more consistent with the qualitative discussions of Bawendi *et al.*[22] and Colvin and co-workers,[31] in which it is proposed that a highly localized intrinsic surface state would, for some range of sizes, be resonant with the interior exciton state, and strong mixing would result. The eigenstate of the system would then have strong dipolar character, which would enhance rather than diminish the polar coupling to lattice vibrations. These eigenstates would be dramatically different from the idealized "particle in a spherical well" wave functions.

Other experiments and recent theoretical considerations have confirmed that the initially prepared state of the system does not reflect characteristics of ideal spherical symmetry. Figure 8 shows a comparison of the photon-echo data of Table I with resonance Raman measurements on the same systems. In this figure, we have used our measured values of Δ and T_2 to calculate the expected ratio of the integrated area of the first Raman overtone peak (at ~420 cm^{-1}) to the area of the Raman fundamental (at ~210 cm^{-1}). It is clear from Fig. 8 that the two experiments are consistent in their measurements of the symmetry of the excited-state charge distribution. In addition, electroabsorption measurements have indicated[31] that there is a dipole moment in the excited state of these nanocrystals, and that the magnitude of this dipole moment peaks near 40-Å diameter, which is in approximate agreement with the results shown here. Raman depolarization measurements have also supported these conclusions.[13,65] Other groups[66] have reported similar effects observed in fluorescence, although only below 10 K. The Raman, photon echo, and electroabsorption measurements taken together are strong evidence that the excited-state charge distribution is *not* well described by "particle in an infinite spherical well" wave functions. Rather, the presence of intrinsic surface states strongly perturbs these eigenstates and cannot be neglected in any realistic treatment of the electronic properties of these materials. Recent theoretical work[67] has begun to address these issues, and such treatments are expected to contribute valuable information on the nature of resonant surface mixing.

D. Temperature dependence

In order to understand the various contributions to electronic dephasing in the nanocrystals, we have measured the photon-echo signals as a function of temperature for several samples. Figure 9 is a summary of this data, in which we show the echo decay rate (the inverse of the measured slope as a function of t_{12} when $\omega t_{13}=2\pi$) as a function of temperature. The zero-temperature decay rates show a strong size dependence; this is evident from the data of Fig. 6. The sensitivity of the dephasing rate to temperature is also size dependent, with the smaller nanocrystals exhibiting the most pronounced temperature dependence. The origin of this temperature effect can be explained by the coupling of the exciton to low-frequency (~5–50 cm^{-1}) vibrational modes which may be either confined (i.e., internal) acoustic vibrations, confined transverse-optical modes, or surface modes.

A confined transverse-optical mode has been observed at 90 cm^{-1} using transient absorption spectroscopy in nanocrystals of PbS.[35] Confined acoustic modes have been observed by low-frequency Raman scattering in a

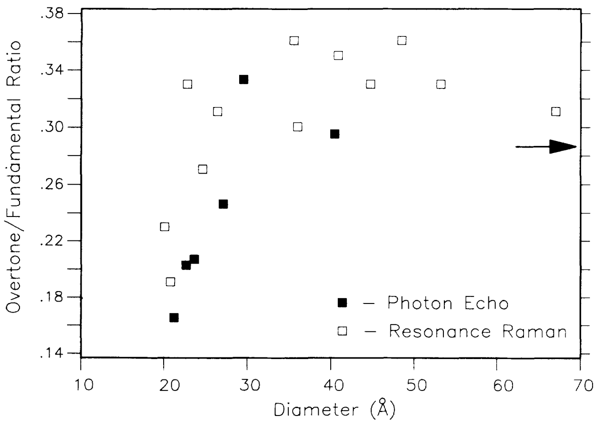

FIG. 8. Calculated values of the ratio of the integrated intensities of the resonance Raman overtone (2 LO) to the fundamental (1 LO), using the data from Table I. Also shown are the measured overtone/fundamental ratios, from Ref. 13. The arrow indicates the bulk value, calculated using the values reported in Table I for bulk CdSe.

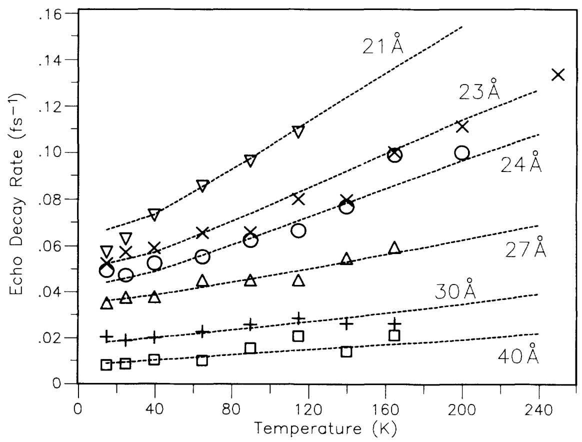

FIG. 9. Temperature dependence of the echo decay rate (inverse of the slope of the echo decay) with $\omega t_{13}=2\pi$ for suppression of the quantum beat. Mean diameters of the nanocrystals are shown. The dashed lines are the predicted temperature dependences using the model discussed in the text. At high temperatures ($T>100$ K), the slopes of these lines are proportional to $g_a\omega_a^3$.

number of nanocrystalline systems, including $MgCr_2O_4$,[68] silver,[69] germanium,[70] and CdS.[71] The frequencies of these acoustic modes shift with particle radius as $\omega \sim 1/R$, in accordance with the theory of Lamb.[72] However, there exists no quantitative experimental measure of the exciton–acoustic-mode-coupling strength, and in particular how this coupling varies with particle size. The deformation potential, which mediates the interaction between the exciton and the acoustic vibrations of the nanocrystal, is a nonpolar coupling. Schmitt-Rink, Miller, and Chemla[63] predicted that confinement of the long-wavelength vibrational modes would result in enhanced nonpolar coupling to the exciton. More recently, Nomura and Kobayashi[73] have performed a detailed calculation of this effect, in which they used confined particle-in-a-sphere wave functions to describe the electron and hole, a continuum approximation to model the vibrational modes of the sphere, and a deformation-potential Hamiltonian appropriate for the wurtzite crystal structure[74] to calculate the coupling constant as a function of particle radius. They determined that the coupling constant g varied roughly as R^{-2}. That is, the deformation-potential coupling should increase dramatically as the size of the nanocrystal decreases. Takagahara[75] has also recently treated this problem, and obtained good theoretical agreement with the data of Ref. 38.

In order to quantify our temperature-dependence data, it is necessary to make some simplifying assumptions about the mode structure of the low-frequency vibrations which are contributing to electronic dephasing. From the experiments on similar systems and from theoretical considerations, it seems likely that no single mode is the dominant factor in determining the dephasing rate. Confined longitudinal and transverse acoustic modes, surface modes, and low-frequency vibrations of the host polymer all could contribute to the decay of the echo. This collection of low-frequency vibrations modulates the electronic transition in much the same way as the optical mode. However, the commensurate period of these vibrations is long compared to other decay mechanisms. Moreover, the confined acoustic modes seem to have damping times which are comparable to their vibrational periods.[71] As result, the low-frequency modes are more accurately described as an "acoustic-mode heat bath," which modulates the transition energy in a stochastic (rather than periodic) fashion.[76] The coupling of this heat bath to the excitonic state can then be parametrized using standard methods from molecular spectroscopy.[77] In particular, we may model the action of the heat bath as a coupling to a single low-frequency mode. This single low-frequency (or "acoustic") mode is not meant to represent an actual vibrational mode of the system, but only to quantify the effect of the coupling to a large number of low-frequency oscillations. We then have two parameters which describe the temperature dependence of the echo decay rate; they are the frequency and coupling parameter of the acoustic mode, ω_a and g_a. The parameter g_a is equivalent to $\frac{1}{2}\Delta_a^2$, where Δ_a is the (dimensionless) displacement of the harmonic acoustic mode. From Eq. (1), we can see how the temperature dependence of the echo decay rate depends on these parameters. If we let $\Phi(t_{12},t_{13})\rightarrow 1$ and $\omega t_{13}=2\pi$, then the natural log of the signal in the presence of *two* modes (the LO mode and the acoustic mode) is given by

$$\ln[S(t_{12},t_{13})] = -8g_a[n(\omega_a)+\tfrac{1}{2}](1-\cos\omega_a t_{12}) \times (1-\cos\omega_a t_{13}) - \frac{4t_{12}}{T_2} - \frac{2t_{13}}{T_1} . \quad (3)$$

We make the additional approximations that the frequency ω_a is low enough that $\omega_a t_{12} \ll 1$ and $\omega_a t_{13} \ll 1$, and also $\hbar\omega_a < k_B T$. In this case, $n(\omega_a) \rightarrow k_B T/\hbar\omega_a$, and we may expand the cosines in Eq. (3), resulting in

$$\begin{aligned}\ln[S(t_{12},t_{13})] &\approx -8g_a\left[\frac{k_B T}{\hbar\omega_a}+\frac{1}{2}\right]\left[\frac{\omega_a^4 t_{12}^2 t_{13}^2}{4}\right] - \frac{4t_{12}}{T_2} - \frac{2t_{13}}{T_1} \\ &= -[A + B(k_B T)(g_a\omega_a^3)] , \end{aligned} \quad (4)$$

where A and B are numerical constants quadratic in t_{12} and t_{13}. In our experiments, we cannot measure either g_a or ω_a, but only the slope of the echo decay rate versus temperature. In the high-temperature limit, the echo decay is determined by the product $g_a\omega_a^3$. This is verified by our simulations, in which we can trade off g_a against ω_a. As long as the product $g_a\omega_a^3$ is preserved, the fits shown in Fig. 9 do not change, at least for $k_B T > \hbar\omega_a$. Therefore, this product is a reasonable parameter with which to compare the data to a theoretical analysis of the coupling. We have calculated the expected behavior of the deformation-potential coupling, following the procedure of Nomura and Kobayashi.[73] This calculation assumes that the confining potential at the nanocrystal surface is infinite and spherical, and uses the confined electron and hole wave functions of Ekimov *et al.*[45] The deformation-potential Hamiltonian[74] and the wave functions describing the confined phonon mode[73] are taken from the literature. The result is shown in Fig. 10, in which the experimentally determined values of $g_a\omega_a^3$ are compared to calculated values. The agreement is surprisingly good, considering that the electron and hole wave functions used in the theory are quite different from the actual wave functions of the excited states of the nanocrystal, as discussed above. The dashed line in Fig. 10 shows the behavior of $1/R^5$, which is the approximate behavior expected, given that $\omega_a \sim 1/R$ and $g_a \sim 1/R^2$.

We have made the assumption that the entire temperature dependence can be attributed to the presence of low-frequency vibrations coupled to the exciton, which become thermally populated as the temperature increases. Other possible explanations for the temperature-dependent broadening have been discussed in the literature, most notably a thermally induced surface trapping. The acoustic-mode-coupling picture, though by no means the only explanation for the observed temperature dependence, is certainly the simplest one. With this assumption, we can predict the low-temperature contribution to the dephasing arising from the zero-point fluctuations of these modes. By subtract-

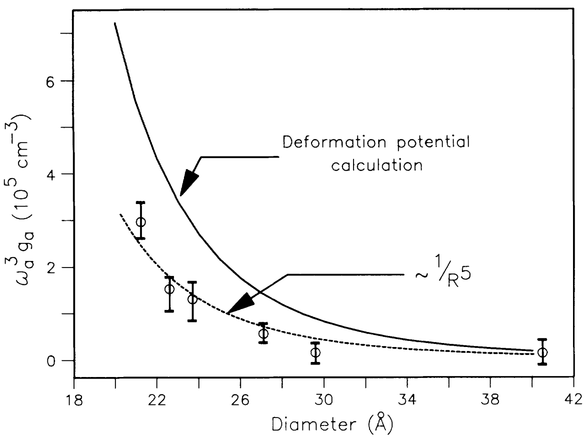

FIG. 10. Experimentally measured values of $g_a\omega_a^3$, as a function of particle diameter. Also shown is the deformation-potential calculation described in the text. The dashed line is proportional to $1/R^5$, the approximate scaling behavior of this parameter.

ing this contribution from the dephasing at low temperatures, we are left with a residual dephasing rate, arising from all other temperature-independent scattering processes. This completes the analysis, as all of the important factors leading to electronic dephasing have been accounted for.

V. CONCLUSION

Semiconductor nanocrystals have become the prototype for solid-state systems which exhibit three-dimensional quantum confinement. They afford a unique opportunity to investigate the properties of matter as it grows from a molecular limit, consisting of only a few unit cells, to a solid system with long-range translational symmetry. We have used the femtosecond photon-echo technique as a direct probe of the electronic properties of these materials. Using this direct measure of electronic dephasing, we have separated the various ultrafast scattering or decay channels contributing to the homogeneous linewidths. By measuring the dephasing rate as a function of both nanocrystal size and temperature, we are able to distinguish between those processes which are inexorably linked to the quantum-confined nature of the excitation and those which are not. Our measurements indicate how the time scales of the various dynamical processes change as a function of the size of the nanocrystal. This gives direct information about the strengths of the excitonic coupling to the lattice, and about the ultrafast excited-state lifetime. These studies of the femtosecond dephasing of the quantum-confined exciton in CdSe nanocrystals have led us to form a more complete description of the dynamics of the optically prepared excited state. We can now answer some of the outstanding questions about the quantum size dependence of the electronic and optical properties of semiconductors.

From the femtosecond three-pulse photon-echo experiments, we conclude that the electronic dephasing and therefore the homogeneous linewidth can be attributed principally to three dynamical processes, all of which are size dependent. These three processes do not all originate from the quantum-confined nature of the electronic excitation. Consequently, this division is important for an understanding of the fundamental physics behind the confinement-induced line broadening observed here and in other experiments.[20,66]

The first mechanism contributing to dephasing is the coupling to a heat bath of low-frequency vibrational modes of the nanocrystal. This mechanism is strongly temperature dependent, leading to line broadening that grows roughly linearly with temperature. As a consequence, acoustic-mode coupling dominates the linewidth at room temperature, leading to a homogeneous width that is an appreciable fraction of the inhomogeneous width in these samples. This is consistent with the fact that it is very difficult to observe spectral hole burning at room temperature.[16] Even at low temperatures, phonon broadening due to low-frequency modes adds a significant contribution (20–35 %) to the homogeneous linewidth.

The second mechanism is the lifetime effect, which corresponds to fast decay of the initial state into some other electronic configuration which is less strongly coupled to the ground state. This results in a fast partial recovery of the bleach signal, and is found to be largely insensitive to the temperature of the sample. This change of state is found to be strongly size dependent, which suggests that it may result from trapping to a localized surface state. The time scale of this process ranges from 400 fs in the smallest samples up to roughly 8 ps in the largest. A change of state must necessarily dephase the excitation, so this lifetime process contributes to the homogeneous linewidth. If the trapping is driven by a simple overlap between an interior wave function and a localized surface state, then we expect that the trapping rate should vary roughly as the ratio of the surface area to the volume of

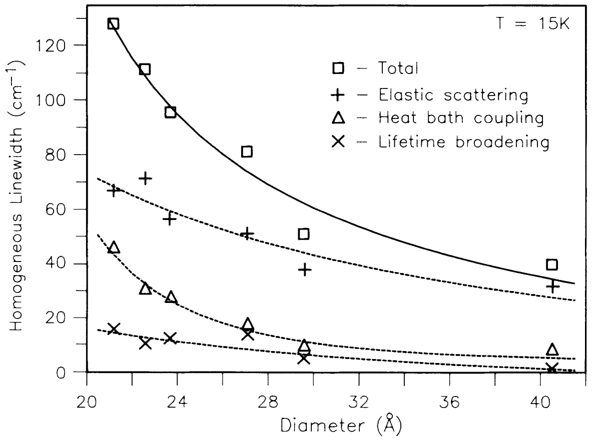

FIG. 11. Measured low-temperature homogeneous linewidth of CdSe nanocrystals, as a function of diameter. The three most important contributing mechanisms to this linewidth are also displayed. The dashed lines show the best fits to $1/R$ (for the lifetime broadening and the elastic scattering, symbols × and +) and $1/R^5$ (for the heat bath coupling, symbol Δ). The solid line through the total linewidth (squares) is the sum of the three dashed lines.

the nanocrystal. This trapping rate ought to be influenced by variations in the surface derivitization and by the host environment (e.g., polymer vs glass).

Finally, there is a contribution to the dephasing which is independent of temperature and which does not lead to a change in the transient bleach signal. This contribution depends on the size of the nanocrystal, and could be caused by elastic scattering from impurity or crystalline defect sites. The effective density of surface scattering sites should vary roughly as the surface-to-volume ratio of the nanocrystal, which might explain the size dependent of this dephasing mechanism.

These results are summarized in Fig. 11, in which the homogeneous linewidth (at 15 K) of the nanocrystals is plotted as a function of particle diameter. Also shown are the three important contributions to that linewidth. We have neglected the small contribution arising from the vibrational damping of the LO-phonon mode. Note that all three of the contributing factors increase with decreasing particle size. The dashed lines show the best fits to $1/R$ (for the lifetime broadening and the elastic scattering, symbols $\times$ and $+$) and to $1/R^5$ (for the heat bath coupling, symbol Δ). The solid line through the total linewidth (squares) is simply the sum of the three dashed lines.

Numerous studies of the homogeneous linewidth of nanocrystal samples have been performed in recent years, primarily using hole burning techniques. However, due to the difficulties associated with interpreting such measurements, no clear division between the various important dephasing processes has been drawn. The femtosecond photon-echo measurements presented here have enabled us to distinguish between those dephasing mechanisms which are intrinsic to quantum-confined systems and those which could be influenced by the surface passivation, crystalline quality or host environment.

ACKNOWLEDGMENTS

We wish to acknowledge the contributions of Dr. W. T. Pollard, who wrote the bulk of the computer code used for the numerical simulations presented in this work. We also wish to thank C. J. Bardeen for helpful discussions. J.J.S. wishes to acknowledge the support of the AT&T Foundation. V.L.C. thanks the Newport Research Corporation for support. A.P.A. acknowledges support from the Alfred P. Sloan Foundation. This work was supported by the U.S. Department of Energy under Contract No. DE-AC0376SF00098.

---

[*] Present address: Room 4C-428, AT&T Bell Laboratory, 101 Crawfords Corner Rd., Holmdel, NJ 07733.

[1] R. K. Jain and R. C. Lind, J. Opt. Soc. Am. **73**, 647 (1983); P. Roussignol, D. Ricard, J. Lukasik, and C. Flytzanis, J. Opt. Soc. Am. B **4**, 5 (1987); D. W. Hall and N. F. Borrelli, J. Opt. Am. B **5**, 1650 (1988); L. H. Acioli, S. L. Gomes, J. R. Rios Leite, and C. B. De Araujo, IEEE J. Quantum Electron. **26**, 1277-1284 (1990); Y. Wang, Acc. Chem. Res. **24**, 133-139 (1991); T. Tokizaki, H. Akiyama, M. Takaya, and A. Nakamura, J. Cryst. Growth **117**, 603 (1992).

[2] D. S. Chemla, D. A. B. Miller, P. W. Smith, A. C. Gossard, and W. Wiegmann, IEEE J. Quantum Electron. **20**, 265 (1984).

[3] D. S. Chemla and D. A. B. Miller, J. Opt. Soc. Am. B **2**, 1155 (1985).

[4] S. Schmitt-Rink, D. S. Chemla, and D. A. B. Miller, Phys. Rev. B **32**, 6601 (1985).

[5] F. C. Spano and S. Mukamel, Phys. Rev. A **40**, 5783 (1989).

[6] L. E. Brus, J. Chem. Phys. **80**, 4403 (1984).

[7] R. Rossetti, R. Hull, J. M. Gibson, and L. E. Brus, J. Chem. Phys. **82**, 552 (1985).

[8] N. Peyghambarian, B. Fluegel, D. Hulin, A. Migus, M. Joffre, A. Antonetti, S. W. Kock, and M. Lindberg, Quantum Electron. **25**, 2516 (1989).

[9] J. Bowen Katari, V. L. Colvin, and A. P. Alivisatos, Phys. Chem. (to be published).

[10] C. B. Murray, D. J. Norris, and M. G. Bawendi, J. Am. Chem. Soc. **115**, 8706 (1993).

[11] K. Misawa, H. Yao, T. Hayashi, and T. Kobayashi, J. Chem. Phys. **94**, 4131 (1991).

[12] W. L. Wilson, P. F. Szajowski, and L. E. Brus, Science **262**, 1242 (1993).

[13] J. J. Shiang, R. K. Grubbs,and A. P. Alivisatos (unpublished).

[14] M. A. Olshavsky, A. N. Goldstein, and A. P. Alivisatos, J. Am. Chem. Soc. **112**, 9438 (1990).

[15] H. Uchida, C. J. Curtis, P. V. Kamat, K. M. Jones, and A. J. Nozik, J. Phys. Chem. **96**, 1156 (1992).

[16] A. P. Alivisatos, A. L. Harris, N. J. Levinos, M. L. Steigerwald, and L. E. Brus, J. Chem. Phys. **89**, 4001 (1988).

[17] P. Roussignol, D. Ricard, C. Flytzanis, and N. Neuroth, Phys. Rev. Lett. **62**, 312 (1989).

[18] M. G. Bawendi, W. L. Wilson, L. Rothberg, P. J. Carroll, T. M. Jedju, M. L. Steigerwald, and L. E. Brus, Phys. Rev. Lett. **65**, 1623 (1990).

[19] Y. Masumoto, T. Wamura, and A. Iwaki, Appl. Phys. Lett. **55**, 2535 (1989).

[20] T. Wamura, Y. Masumoto, and T. Kawamura, Appl. Phys. Lett. **59**, 1758 (1991).

[21] C. Spiegelberg, F. Henneberger, and J. Puis, Superlatt. Microstruct. **9**, 487 (1991).

[22] M. G. Bawendi, P. J. Carroll, W. L. Wilson, and L. E. Brus, J. Chem. Phys. **96**, 946 (1992).

[23] M. O'Neil, J. Marohn, and G. McLendon, Chem. Phys. Lett. **168**, 208 (1990).

[24] T. Inokuma, T. Arai, and M. Ishikawa, Phys. Rev. B **42**, 11 093 (1990).

[25] T. Itoh and M. Furumiya, J. Lumin. **48&49**, 704 (1991).

[26] V. S. Dneprovskii, A. L. Efros, A. I. Ekimov, V. I. Klimov, I. A. Kudriavtsev, and M. G. Novkov, Solid State Commun. **74**, 555 (1990).

[27] A. P. Alivisatos, T. D. Harris, P. J. Carroll, M. L. Steigerwald, and L. E. Brus, J. Chem. Phys. **90**, 3463 (1989).

[28] J. J. Shiang, S. H. Risbud, and A. P. Alivisatos, J. Chem. Phys. **98**, 8432 (1993).

[29] M. C. Klein, F. Hache, D. Ricard, and C. Flytzanis, Phys. Rev. B **42**, 11 123 (1990).

[30] A. Tanaka, S. Onari, and T. Arai, Phys. Rev. B **45**, 6587 (1992); A. Tanaka, S. Onari, and T. Arai, J. Phys. Soc. Jpn.

61, 4222 (1992); J. J. Shiang, A. N. Goldstein, and A. P. Alivisatos, J. Chem. Phys. **92**, 3232 (1990); X. S. Zhao, J. Schroeder, F. D. Persans, and T. G. Bilodeau, Phys. Rev. B **43**, 12 580 (1991); A. A. Baranov, Y. S. Bobovich, and V. I. Petrov, Solid State Commun. **83**, 957 (1992).

[31] V. L. Colvin and A. P. Alivisatos, J. Chem. Phys. **97**, 730 (1992); V. L. Colvin, K. L. Cummingham, and A. P. Alivisatos, J. Chem Phys. **97**, 730 (1992); V. L. Colvin, K. L. Cunningham, and A. P. Alivisatos, *ibid.* (to be published).

[32] T. Sekikawa, H. Yao, T. Hayashi, and T. Lobayashi, Solid State Commun. **83**, 969 (1992); A. I. Ekimov, A. L. Efros, T. V. Shubina, and A. P. Skvortsov, J. Lumin. **46**, 97 (1990); F. Hache, D. Ricard, and C. Flytzanis, Appl. Phys. Lett. **55**, 1504 (1989).

[33] K. Shum, W. B. Wang, R. R. Alfano, and K. M. Jones, Phys. Rev. Lett. **68**, 3904 (1992).

[34] Y. E. Lozovik, Y. A. Matveets, A. G. Stepanov, V. M. Farztdinov, S. V. Chekanin, and A. P. Yartsev, Pis'ma Zh. Eksp. Teor. Fiz. **52**, 851 (1990) [JETP Lett. **52**, 221 (1990)].

[35] J. L. Machol, F. W. Wise, R. C. Patel, and D. B. Tanner, Phys. Rev. B **48**, 2819 (1993).

[36] D. J. Norris, M. Nirmal, C. B. Murray, A. Sacra, and M. G. Bawendi, Z. Phys. D **26**, 355 (1993).

[37] P. C. Becker, H. L. Fragnito, C. H. Brito Cruz, R. L. Fork, J. E. Cunningham, J. E. Henry, and C. V. Shank, Phys. Rev. Lett. **61**, 1647 (1988).

[38] R. W. Schoenlein, D. M. Mittleman, J. J. Shiang, A. P. Alivisatos, and C. V. Shank, Phys. Rev. Lett. **70**, 1014 (1993).

[39] J. R. Sachleben, E. W. Wooten, L. Emsley, A. Pines, V. L. Colvin, and A. P. Alivisatos, Chem. Phys. Lett. **198**, 431 (1992).

[40] R. Rossetti, J. L. Ellison, J. M. Gibson, and L. E. Brus, J. Chem. Phys. **80**, 4464 (1984); M. L. Steigerwald, A. P. Alivisatos, J. M. Gibson, T. D. Harris, R. Kortan, A. J. Muller, A. M. Thayer, T. M. Duncan, D. C. Douglass, and L. E. Brus, J. Am. Chem. Soc. **110**, 3046 (1988); M. G. Bawendi, A. R. Kortan, M. L. Steigerwald, and L. E. Brus, J. Chem. Phys. **91**, 7282 (1989); B. Champagnon, J. Appl. Phys. **73**, 2775 (1993).

[41] W. H. Knox, M. C. Downer, R. L. Fork, and C. V. Shank, Opt. Lett. **9**, 552 (1984).

[42] R. L. Fork, C. H. Brito Cruz, P. C. Becker, and C. V. Shank, Opt. Lett. **12**, 483 (1987).

[43] G. Boyer, M. Franco, J. P. Chambaret, A. Migus, A. Antonetti, P. Georges, F. Salin, and A. Brun, Appl. Phys. Lett. **53**, 823 (1988).

[44] R. W. Schoenlein, J.-Y. Bigot, M. T. Portella, and C. V. Shank, Appl. Phys. Lett. **58**, 801 (1991).

[45] A. I. Ekimov, F. Hache, M. C. Schanne-Klein, D. Ricard, C. Flytzanis, I. A. Kudryavtsev, T. V. Yazeva, A. V. Rodina, and A. L. Efros, J. Opt. Soc. Am. B **10**, 100 (1993).

[46] L. G. Rowan, E. L. Hahn, and W. B. Mims, Phys. Rev. **137**, A61 (1965); W. B. Mims, Phys. Rev. B **5**, 2409 (1972); **6**, 3543 (1972).

[47] S. Nakanishi, O. Tamura, T. Muramoto, and T. Hashi, Jpn. J. Appl. Phys. **19**, L57 (1980); M. K. Kim and R. Kachru, Phys. Rev. B **44**, 9826 (1991); M. Mitsunaga, R. Yano, and N. Uesugi, *ibid.* **45**, 12 760 (1992).

[48] C. J. Bardeen and C. V. Shank, Chem. Phys. Lett. **203**, 535 (1993).

[49] W. T. Pollard, S.-Y. Lee, R. A. Mathies, J. Chem. Phys. **92**, 4012 (1990).

[50] G. Stock and W. Domcke, J. Chem. Phys. **93**, 5496 (1990).

[51] W. T. Pollard, S. L. Dexheimer, Q. Wang, L. A. Peteanu, C. V. Shank, and R. A. Mathies, J. Phys. Chem. **96**, 6147 (1992).

[52] Y. J. Yan and S. Mukamel, J. Chem. Phys. **94**, 179 (1991).

[53] S. Mukamel and R. F. Loring, J. Opt. Soc. Am. B **3**, 595 (1986).

[54] E. J. Heller, J. Chem. Phys. **62**, 1544 (1975).

[55] W. B. Bosma, Y. J. Yan, and S. Mukamel, Phys. Rev. A **42**, 6920 (1990).

[56] Y. J. Yan and S. Mukamel, J. Chem. Phys. **89**, 5160 (1988).

[57] K. Duppen and D. A. Wiersma, J. Opt. Soc. Am. B **3**, 614 (1986).

[58] Y. Wang, A. Suna, J. McHugh, E. F. Hilinski, P. A. Lucas, and R. D. Johnson, J. Chem. Phys. **92**, 6927 (1990).

[59] W. Hoheisel, V. L. Colvin, C. Johnson, and A. P. Alivisatos (unpublished).

[60] A. B. Myers and R. A. Mathies, in *Biological Applications of Raman Spectroscopy,* edited by T. G. Spiro (Wiley, New York, 1987), pp. 1–58.

[61] T. Joo and A. C. Albrecht, Chem. Phys. **173**, 17 (1993).

[62] U. Woggon, S. Gaponenko, W. Langbein, A. Uhrig, and C. Klingshirn, Phys. Rev. B **47**, 3684 (1993).

[63] S. Schmitt-Rink, D. A. B. Miller, and D. S. Chemla, Phys. Rev. B **35**, 8113 (1987).

[64] S. Nomura and T. Kobayashi, Phys. Rev. B **45**, 1305 (1992).

[65] J. J. Shiang, I. M. Craig, and A. P. Alivisatos, Z. Phys. D **26**, 358 (1993).

[66] M. Nirmal, C. B. Murray, D. J. Norris, and M. G. Bawendi, Z. Phys. D **26**, 361 (1993).

[67] N. Hill and B. Whaley, J. Chem. Phys. **99**, 3707 (1993).

[68] E. Duval, A. Boukenter, and B. Champagnon, Phys. Rev. Lett. **56**, 2052 (1986).

[69] M. Fujii, T. Nagareda, S. Hayashi, and K. Yamamoto, Phys. Rev. B **44**, 6243 (1991); M. Fujii, T. Nagareda, S. Hayashi, and K. Yamamoto, J. Phys. Soc. Jpn. **61**, 754 (1992); G. Mariotto, M. Montagna, G. Viliani, E. Duval, S. Lefrant, E. Rzepka, and C. Mai, Europhys. Lett. **6**, 239 (1988).

[70] N. N. Ovsyuk, E. B. Gorokhov, V. V. Grishchenko, and A. P. Shebanin, Pis'ma Zh. Eksp. Teor. Fiz. **47**, 248 (1988) [JETP Lett. **47**, 298 (1988)].

[71] A. Tanaka, S. Onari, and T. Arai, Phys. Rev. B **47**, 1237 (1993).

[72] H. Lamb, Proc. London Math. Soc. **13**, 189 (1882).

[73] S. Nomura and T. Kobayashi, Solid State Commun. **82**, 335 (1992).

[74] G. E. Pikus, Zh. Eksp. Teor. Fiz. **41**, 1507 (1961) [Sov. Phys. JETP **14**, 1075 (1962)].

[75] T. Takagahara, Phys. Rev. Lett. **71**, 3577 (1993).

[76] If the low-frequency spectrum is comprised of a small number of well-defined modes, and if all other dephasing processes are slow compared to the vibrational periods of these modes, then the acoustic modes would be expected to periodically modulate the polarization, in analogy with the LO phonon. In this case, the contribution to electronic dephasing from these low-frequency modes would be a reversible process. We have observed no evidence of this effect.

[77] J. Yu and M. Berg, J. Chem. Phys. **96**, 8741 (1992).

[78] H. Schwab, C. Dornfeld, E. O. Gobel, J. M. Hvam, C. Klingshirn, J. Kuhl, V. G. Lyssenko, F. A. Majumder, G. Noll, J. Nunnenkamp, K.-H. Pantke, R. Renner, A. Reznitsky, U. Siegner, H. E. Swoboda, and C. Weber, Phys. Status Solidi B **72**, 479 (1992).